JOURNAL OF
Optical Communications
and Networking

Impairment- and fragmentation-aware, energy-efficient dynamic RMSCA for SDM-EONs

JAYA LAKSHMI RAVIPUDI* AND MAÏTÉ BRANDT-PEARCE

Charles L. Brown Department of Electrical and Computer Engineering, University of Virginia, Charlottesville, Virginia 22904, USA
**jr3vz@virginia.edu*

Received 6 February 2023; revised 12 April 2023; accepted 21 April 2023; published 4 August 2023

This paper presents a routing, modulation, spectrum, and core allocation (RMSCA) algorithm for space-division multiplexing-based elastic optical networks (SDM-EONs). A network state-dependent route and core selection method is proposed using a multi-attribute decision-making method based on the analytic hierarchy process (AHP) and preference ranking organization method for enrichment evaluations (PROMETHEE) methods. This systematic resource allocation allows the network designer to choose which resources are most valuable. It is followed by a spectrum allocation algorithm using a weighted score function to rate and select the best spectrum blocks. Physical layer impairments, including inter-core cross talk, amplified spontaneous emission, and Kerr fiber nonlinearities, are considered alongside fragmentation and energy consumption. The proposed RMSCA approach is compared with published benchmarks incorporating quality of transmission constraints and evaluated on two network topologies, NSFNET (7- and 12-core multicore fiber links) and COST. It is shown to be superior in terms of blocking probability, bandwidth blocking probability, network fragmentation, and energy consumption compared to standard and published benchmarks.

https://doi.org/10.1364/JOCN.486874

1. INTRODUCTION

Optical transmission systems and networks are vital to the worldwide communications infrastructure. The rising number of gadgets, social media and video streaming users, and machine-to-machine communications drives the need to use communication networks efficiently [1]. Over the last few years, elastic optical networks (EONs) have been widely researched due to their more efficient spectrum utilization than wavelength-division multiplexing (WDM) optical networks. EONs have a finer frequency grid of widths 12.5 GHz or 6.25 GHz instead of 50 GHz of WDM. Hence, EONs generate elastic optical paths that divide the available spectrum flexibly and allocate the available resources in a network according to the traffic demands of the users, leading to efficient utilization of fiber bandwidth (BW). However, the currently deployed single-core fiber capacity is nearly exhausted. Possible solutions to this problem include using extended frequency bands [2], multi-fiber links, and multicore fiber (MCF) links [3]. MCFs exploit the spatial domain by having spatially separated cores in a fiber, creating a space-division multiplexed EON (SDM-EON). Frequency band extension can increase the network capacity by only a small factor compared with exploiting MCFs. Hence, the network will eventually need to rely on more transmission dimensions as available in SDM-EON.

The task of selecting a route and contiguous spectral slots on each link of the route while avoiding frequency overlapping for a given traffic demand is called the routing and spectrum assignment (RSA) problem in EONs, or RMSA if adaptive modulation is considered. It is an NP-hard problem [4]. RMSA becomes routing, modulation, spectrum, and core allocation (RMSCA) when the resource allocation algorithm must also select a core in MCF-enabled SDM-EONs. The traffic demands may be static (i.e., a fixed or offline traffic matrix) or dynamic (i.e., time-varying traffic). Resource allocation algorithms for dynamic traffic work in real time and need to be faster.

Some network aspects worth considering in RMSCA algorithm design are fragmentation, physical layer impairments (PLIs), and energy consumption. The dynamic setting and tearing up of traffic connections can lead to BW fragmentation: the random occurrence of scattered and varying-sized spectral gaps that makes it challenging to allocate contiguous and continuous spectral blocks along an entire route. This results in inefficient spectrum use and traffic blocking. Fragmentation is unavoidable but can be managed by proper RMSCA decisions to minimize the effect.

PLIs degrade the signal's quality of transmission (QoT) and limit the transmission reach. Linear effects include amplified spontaneous emission (ASE) and cross talk (XT), and nonlinear impairments (NLIs) include self-phase modulation (SPM) and cross-phase modulation (XPM). Inter-core XT is the unwanted signal interaction between signals propagating on adjacent fiber cores and is an added significant challenge

1943-0620/23/090D10-13 Journal © 2023 Optica Publishing Group

when using MCFs compared to single-core EONs. However, minimizing XT can lead to network fragmentation, resulting in under-utilization. XT minimization prefers inter-signal spacing in the spectral assignment phase to avoid signal overlap. In contrast, fragmentation mitigation demands compact spectral assignment to avoid unnecessary spectrum gaps to make it easier to satisfy continuity and contiguity constraints. Hence, it becomes important to view the two issues collectively while allocating the spectrum.

SDM-EONs offer higher capacity due to multiple cores, yet this also increases energy consumption because of more network elements such as BW variable transponders (BVTs), BW variable optical cross-connects (OXCs), and erbium-doped fiber amplifiers (EDFAs). Hence, keeping energy usage to a minimum while solving the RMSCA problem is another essential aspect to consider [5–8].

Keeping these aspects in mind, this paper proposes a heuristic dynamic RMSCA algorithm that reduces the probability of a connection request being blocked. It is achieved by using a multi-attribute decision-making (MADM) method to choose the core and route and a weighted score function to select the spectral block for transmission. Both of these algorithms are designed to minimize the effects of fiber impairments on the signal QoT while maintaining lower network fragmentation and energy consumption than the baseline approaches.

The rest of this paper is organized as follows. Section 2 summarizes the current literature in this area and highlights our paper's novel contributions. Section 3 gives the system description and the evaluation metrics. Section 4 elaborates on the MADM technique and its adaptation for routing. Section 5 details the proposed RMSCA algorithm. Finally, Section 6 gives the performance evaluation of the algorithm, followed by conclusions in Section 7.

2. LITERATURE REVIEW AND PAPER CONTRIBUTIONS

Several research works can be found in the literature on solving the RMSCA problem in SDM-EONs. In [6], an RSCA algorithm for energy-efficient architecture on-demand modules was proposed; these modules provide flexibility of SDM-EON architectures but suffer from high power consumption. In [9], the authors proposed an RSCMA algorithm ("M" here stands for mode) where they included both MCF and multimode fibers, and XT was the only impairment considered. In [10], a static RCSA problem was solved using mixed integer linear programming (MILP) models for XT-aware and XT-unaware cases; the dynamic traffic case was not considered. In [11], an RMSCA scheme was proposed to reduce the wasted spectrum and to exploit path diversity, but in this case, the XT was assumed to be negligible. In [12], an energy-efficient RMSCA scheme was proposed using a multipath scheme for survivability. XT was the only PLI considered, and the objective was to improve spectral efficiency during fluctuating traffic without regard to fragmentation. The work of [8], which preceded [7] described above, also considered energy efficiency for static traffic scenarios.

Some recent works solve the RMSCA problem differently by considering aspects of network load balancing, different XT representation and traffic, or a combination of network issues. In [13], SDM-EONs supporting super-channels were considered that allow the usage of frequency slots on neighboring cores to form contiguous spectrum blocks. The RMSCA used a load-balancing strategy and a metric accounting for spatial and spectral fragmentation to minimize the number of wasted slots; impairments, however, were not considered. In [14], the authors devised an effective XT representation model and an RMSCA strategy that minimizes it, but other PLIs were not considered. In [15], the authors proposed an RMSCA scheme based on MILP and a heuristic approach for delay-sensitive multicast traffic; again only XT impairment was considered. In [16], an RMSCA scheme was presented to improve spectrum efficiency while focusing on XT and fragmentation issues. A new modulation format selection method is provided w.r.t. XT-fragmentation reduction. To our knowledge, this is the only paper (except for our own work [17]) that addressed the importance of the combined XT-fragmentation problem. However, other impairments were not included. In [18], a dynamic impairment-aware (DI-aware) RMSCA algorithm was proposed considering XT, ASE, and XPM effects, but not the quite important SPM. The work considered other PLIs (except SPM), unlike most other PLI-aware RMSCA studies, and hence, our work uses this algorithm for benchmarking purposes. In [19], fragmentation-aware RSCA algorithms were proposed using a core classification method for spectrum assignment and a cost function to increase spectrum efficiency. However, impairments were not considered in the design process.

Most XT-aware networking studies compute the worst-case XT levels, i.e., all neighbor cores are considered active [10,20–22]. This approach simplifies the computation but increases the blocking of incoming traffic demands due to conservative XT estimates. On the other hand, computing precise XT levels dynamically, as used in [23,24], can be time consuming. A lesser time-consuming version that considers spectral blocks can be found in [25] and is used in this work. However, these researchers did not consider the network fragmentation and energy consumption aspects.

Almost all of the RMSCA algorithms in the literature use the K-shortest paths (KSP) method for routing. KSP routing based on distance results in the same paths used for any network source–destination pair, irrespective of the network state. This increases link congestion and blocks future traffic requests. In addition, as distance-based KSP focuses only on the shortest paths, the routing part of the RMSCA design does not help tackle other network issues, such as PLIs or fragmentation. Instead of using distance in the path selection, the number of hops or some cost that is a function of link parameters can be employed. In [13], a load-balanced routing method that considers fragmentation is proposed. In [26], traffic-aware routing is performed to choose routes based on the incoming traffic demand, and [27] suggests a fragmentation- and alignment-aware routing for 3D elastic optical networking. However, more relevant network metrics could be incorporated into routing decisions. Using MADM approaches to perform routing using multiple metrics in a systematic manner, as we propose in this paper, has not been previously considered.

Recently, approaches using machine learning (ML) for RMSCA have been explored. In [28], an ML model trained with synthetic traffic estimated a path's acceptability based on XT, fragmentation, and required slots. More features related to impairments and network topology would need to be included to compare their results to our work. In [29], the authors used a deep reinforcement learning approach to solve the RMSCA task. However, only XT impairment was considered. Using ML for RMSCA is an attractive prospect to consider; however, care should be taken to include critical network aspects such as PLIs, fragmentation, and energy consumption. Moreover, obtaining training data that effectively covers network features remains a difficult task and is an active area of research.

Fiber PLIs, specifically the ASE, SPM, and XPM effects, have been widely considered in single-core RMSA algorithms; however, to the best of our knowledge, there are no published RMSCA algorithms that holistically consider these impairments alongside XT, and this paper addresses this gap. There are two reasons it is important to do this. First, these impairments together significantly limit the signal reach, which is a major design aspect of any impairment-aware RMSCA, and hence, considering XT alone is not enough. Second, a higher utilization in one core increases the NLI effects, whereas spreading the traffic over different cores exacerbates the XT. Hence, these factors affect the routing decisions, the required spectrum range and, subsequently, the networking costs.

Table 1 shows the literature works that considered impairments, fragmentation, and energy efficiency aspects. To our knowledge, no works have covered all impairments while including fragmentation and energy consumption issues in performing dynamic resource allocation. Therefore, keeping all the above aspects in mind, the following contributions are made in this paper.

Table 1. Literature on Dynamic Allocation Considering Impairments, Fragmentation, and Energy Efficiency

Related Works	Network Issues Considered			
	Impairments			
	XT	ASE, SPM, XPM	Fragmentation	Energy Efficiency
[5]	✓	—	—	✓
[6]	—	—	✓	✓
[14]	✓	—	✓	—
[15]	✓	—	—	—
[11]	—	—	✓	—
[10]	✓	—	—	—
[9]	—	—	—	—
[12]	✓	—	—	✓
[13]	—	—	✓	—
[16]	✓	—	✓	—
[17]	✓	—	✓	✓
[18]	✓	✓ (except SPM)	—	—
[19]	—	—	✓	—
[21]	✓	—	✓	—
[23]	✓	—	—	—
[24]	✓	—	—	—
[25]	✓	—	—	—
[28]	✓	—	✓	—
[29]	✓	—	—	—
Current paper	✓	✓	✓	✓

- An energy-efficient PLI- and fragmentation-aware dynamic RMSCA is proposed. The PLIs consider ASE, XPM, and SPM effects in addition to XT.
- Our previous work reported in [17], which considered the XT impairment and network fragmentation aspects under the standard KSP routing, is extended in terms of spectrum allocation and routing.
- The routing is improved by including network-dependent parameters in the decisions and applying a new MADM approach. The proposed routing method checks the best path and core combinations while considering multiple network features.
- A weighted score function combining XT, fragmentation, and energy consumption is proposed to rate and select the best spectral block for spectrum allocation.
- The results of the proposed algorithm are compared with standard and published benchmarks on 7- and 12-core-based NSFNET and COST networks.

3. SYSTEM DESCRIPTION AND EVALUATION METRICS

This section describes the PLIs and provides the QoT model used in this work. The network's fragmentation and energy consumption aspects are discussed, accompanied by the corresponding evaluation metrics.

A. Physical Layer Impairments

The QoT of optical signals is degraded by phenomena such as Kerr NLIs and ASE noise occurring during the propagation and detection processes. The NLI is caused by the interaction of nonlinearity and dispersion in the fiber, and the ASE noise is due to EDFAs. These impairments affect the end-to-end QoT, thus limiting the signal's transmission reach. A well-known and widely used PLI estimation model in long-haul transport networks is the so-called Gaussian noise (GN) model, which is a state-dependent (traffic-dependent) model [30].

ASE noise power, $P_{\mathrm{ASE}}^{(e)}$, is modeled as additive Gaussian noise, and for a link e with $N_s^{(e)}$ spans can be computed as

$$P_{\mathrm{ASE}}^{(e)} = N_s^{(e)} \left(e^{\alpha L_s} - 1\right) h \nu \eta_{sp} \Delta f, \tag{1}$$

where α is fiber attenuation; L_s is fiber length per span, i.e., length of the fiber between amplifiers; h is Planck's constant; ν is the optical light frequency; η_{sp} is the spontaneous emission factor; and Δf is the signal BW.

The NLIs considered in this work are SPM and XPM. The closed-form GN model to compute the NLI power generated in the eth optical link with $N_s^{(e)}$ spans at a channel of interest centered at frequency f can be given as

$$P_{\mathrm{NLI}}^{(e)}(f) = P_{\mathrm{ch}}^3 N_s^{(e)} \left(\eta_{\mathrm{XPM}}(f) + \eta_{\mathrm{SPM}}(f)\right), \tag{2}$$

where P_{ch} is the signal power, assumed to be the same for all demands. The procedure to calculate NLI coefficients $\eta_{XPM}(f)$ and $\eta_{SPM}(f)$ can be found in Eqs. (7)–(11) in [31].

XT, an additional impairment in SDM-EON systems, refers to the unwanted interference of lightpath signals propagating in physically adjacent cores. The XT power on a link e for a given lightpath L can be estimated using [25]

$$P_{XT}^{(e)} = P_{ch} \cdot XT_L^{(e)} \tag{3}$$

and

$$XT_L^{(e)} = A_{max}(L, e) \cdot h \cdot \ell^{(e)}, \tag{4}$$

where $\ell^{(e)}$ is the length of the fiber link e, and h is the power-coupling coefficient. $XT_L^{(e)}$ is the XT of the most affected spectral slice of lightpath L on link e, and $A_{max}(L, e)$ is the maximum number of currently active adjacent cores surrounding the spectral block of the core under consideration on link e of lightpath L.

The signal-to-noise ratio (SNR) of a lightpath L is calculated using

$$SNR(f) = \sum_{e \in L} \left(\frac{P_{ch}}{P_{ASE}^{(e)}(f) + P_{NLI}^{(e)}(f) + P_{XT}^{(e)}} \right). \tag{5}$$

In this work, the SNR that the current request would experience if it were to be assigned a particular tentative route is calculated using Eq. (5) and compared with an SNR threshold:

$$SNR(f) > SNR_{th}, \tag{6}$$

where SNR_{th} depends on the modulation format chosen. Also, in addition to satisfying its SNR constraint, the new and about-to-be-provisioned request should not degrade existing requests already provisioned along various links of the tentative route. Hence, the SNR constraint also includes checking their corresponding SNR threshold requirements.

B. Fragmentation

Fragmentation is another cause of blocking in RMSCA due to the creation of spectrum fragments that cannot be used by incoming calls and still satisfy continuity and contiguity constraints, leading to spectrum wastage. The network-wide fragmentation F_{NET} for a network with $|E|$ number of edges can be computed as in [32]:

$$F_{NET} = \frac{\sum_{e \in E} F^{(e)}}{|E|}, \tag{7}$$

where $F^{(e)}$ is the fragmentation on link e computed as the average of core fragmentation over all cores and can be computed as

$$F^{(e)} = \frac{1}{|C|} \sum_{c \in C} F_c^{(e)}, \tag{8}$$

with

$$F_c^{(e)} = \sum_{\gamma_{ec} \in \Gamma_{ec}} \frac{|\gamma_{ec}|}{S} \cdot \ln \frac{S}{|\gamma_{ec}|}. \tag{9}$$

C is the set of cores per link, $|C|$ is the number of cores per link, Γ_{ec} is the set of fragments on link e of core c, $|\gamma_{ec}|$ is the size of fragment γ_{ec}, i.e., number of frequency slots in that fragment, and S is the total number of frequency slots in the C-band. This fragmentation metric is based on the entropy concept and better captures the difference in fragment sizes compared to the general external fragmentation formula [32].

C. Energy Consumption

BVTs typically consume more energy than the other two power-consuming elements, OXCs and EDFAs, while provisioning a traffic request [12]. The energy consumption of a BVT depends on the number of frequency slots used by the request and hence depends on the resource allocation decisions. Longer paths demand more spectral resources and are influenced by chosen modulation formats (Table 1 in [12]). The energy consumption model given by Eqs. (10)–(15) is adapted from [12]. The energy consumed by BVTs to provision the request on a given path L is given by

$$E_{BVT} = \sum_{e \in L} S_m^{(e)} \cdot E_{BVT}(m), \tag{10}$$

where $S_m^{(e)}$ is the total number of spectrum slots allocated to demand r using modulation m on link e. $E_{BVT}(m)$ is the energy consumed by the BVT for a spectral slot using a given modulation format m, which depends on the data rate supported by a frequency slot using modulation format m, $T(m)$, in Gbps, and can be estimated as

$$E_{BVT}(m) = 1.683 \cdot T(m) + 91.333. \tag{11}$$

The energy $E_{OXC}(n)$ consumed by an OXC at node n depends on the node degree $N_d(n)$, add/drop degree β, and some overhead energy. It can be approximated as

$$E_{OXC}(n) = 85 \cdot N_d(n) + \beta \cdot 100 + 150. \tag{12}$$

Hence, the total OXC consumption to accommodate a request on a path L with S available slots is given by

$$E_{OXC} = \sum_{n \in N(L)} \frac{S^{(e,n)}}{S} \cdot E_{OXC}(n), \tag{13}$$

where $S^{(e,n)}$ is the number of occupied slots on link e connecting node n and the next node of lightpath L, and $N(L)$ is the set of nodes of L.

The energy consumed by EDFAs on a link e can be estimated as

$$E_{EDFA}^{(e)} = \left(\frac{\ell^e}{L_s} + 1 \right) \cdot 100, \tag{14}$$

assuming the energy consumed by an amplifier is approximately 100 W [33]. Hence, the total energy consumed by the EDFAs in link spectrum slot $S^{(e)}$ along lightpath L is given as

$$E_{EDFA} = \sum_{e \in L} \frac{S^{(e)}}{S} \cdot E_{EDFA}^{(e)}. \tag{15}$$

The sum of these E_{BVT}, E_{OXC}, and E_{EDFA} is the total energy consumed by a request on path L. And the total network energy consumption (E_{NET}) calculated as the energy consumed by all BVTs, OXCs, and EDFAs use these expressions summed over all active requests.

4. MULTI-ATTRIBUTE DECISION-MAKING

Multi-criteria decision-making is a popular branch of decision-making that falls under the discipline of Operations Research. It is categorized into MADM and multi-objective decision-making (MODM), depending on the domain of the alternatives. MODM methods are preferred when the problem is a decision problem and the decision variables have values in the continuous or integer domain. These methods generally have infinite or many alternatives. However, MADM methods are applied when faced with the problem of selecting the best viable option (or sorting and ranking) from a given finite set of alternatives, as is the case for our RMSCA problem.

Optimization algorithms use an objective criterion to determine the optimal solution. Often in complex problems, simple objective functions cannot be phrased or solved. Heuristic algorithms are then used to weight multiple factors and decide on a viable solution. It is then essential to use scientific methods to structure the problem correctly and arrive at a well-informed decision. In this section, we describe our heuristic yet structured MADM approach to routing and core selection.

MADM methods need alternatives and attributes, and the values of the alternatives are calculated w.r.t. different attributes considered. The attributes influence the alternatives; hence, weights are assigned to them that determine the importance/influence they can have in the decision-making process to achieve a specific goal. What weights to assign to the attributes is the decision maker's choice. Example MADM methods include simple additive weighting (SAW), analytic hierarchy process (AHP), preference ranking organization method for enrichment evaluations (PROMETHEE), technique for order preference by similarity to ideal solution (TOPSIS), compromise ranking method (VIKOR), etc. [34,35].

Of the MADM methods, PROMETHEE is simple to apply, involves less computation, and can handle qualitative and quantitative attributes easily. Hence, in this paper, we use PROMETHEE combined with the AHP method. [36]. PROMETHEE belongs to a category of outranking methods that was introduced by [37] and has been applied in various areas such as banking, workforce planning, water resources, investments, medicine, chemistry, health care, dynamic management, etc., mainly due to its ease of application [37]. PROMETHEE handles the alternatives and attributes in a detailed manner but lacks a systematic way to compute the attribute weights [37]. AHP provides a systematic and practical approach to finding attribute weights and ranking the alternatives [38]. Therefore, to determine the attributes' weights, the present work uses the AHP method, and the same weights are used in PROMETHEE. The steps of the method are outlined below, and a detailed demonstration of the route–core selection process using the proposed AHP-enabled PROMETHEE is given in Section 5.

Table 2. General Form of the Decision Table in MADM

	Attributes			
Alternatives	a_1	a_2	$\cdots$	a_Y
Alt_1	v_{11}	v_{12}	$\cdots$	v_{1Y}
Alt_2	v_{21}	v_{22}	$\cdots$	v_{2Y}
Alt_3	v_{31}	v_{32}	$\cdots$	v_{3Y}
$\vdots$	$\cdots$	$\cdots$	$\ddots$	$\cdots$
Alt_X	v_{X1}	v_{X2}	$\cdots$	v_{XY}

Step 1: Identify the "proper" attributes (or criteria) for the problem

The first step is to create a short list of the alternatives based on the attributes identified. The attribute values can be the already-available data or data estimated by the decision maker. Table 2 shows the general form of the decision table used in MADM methods based on these alternatives–attributes.

Alt_x (for $x = 1, 2, \ldots, X$) denotes alternative x, a_y (for $y = 1, 2, \ldots, Y$) denotes attribute y, and v_{xy} denotes the performance measure used, i.e., the value corresponding to alternative x with respect to attribute y.

Step 2: Decide the attributes' weights using AHP

In this paper, the steps of the AHP are adopted from [35]. Calculating weights involves an important step of forming a relative importance (RI) matrix that denotes the RI of the attributes considered and is determined by the decision maker depending on the goal of the task. AHP provides an RI relations table to quantitatively fill the RI matrix, showing the importance of a particular attribute over another using a standard scale of 1–9, as shown in Table 3, rather than using random intuition. The generic structure of an RI matrix for Y attributes is given as

$$\text{RI} = \begin{array}{c} \text{Attribute} \\ a_1 \\ a_2 \\ \cdots \\ a_Y \end{array} \begin{array}{c} \begin{array}{cccc} a_1 & a_2 & \cdots & a_Y \end{array} \\ \begin{bmatrix} 1 & r_{12} & \cdots & r_{1Y} \\ r_{21} & 1 & \cdots & r_{2Y} \\ \vdots & \vdots & \ddots & \vdots \\ r_{Y1} & r_{Y2} & \cdots & 1 \end{bmatrix} \end{array}, \tag{16}$$

where r_{ij} denotes the RI of attribute i over attribute j with $r_{ij} = 1/r_{ji}$; $r_{ij} = 1$ for $i = j$. Using the degree of importance in Table 3 as either r_{ij} or $1/r_{ij}$, the RI matrix is filled, and the weights are computed. The geometric means for each attribute is computed row-wise in the RI matrix Eq. (16) and then normalized by their sum to get the weights, w_y.

To verify the correctness of the weights found, a consistency ratio (CR) is computed that should be less than 0.1, i.e., $<10\%$, judgment error [36]. The additional steps to verify the weight computations are given as below.

Step A: Compute the vector $M = (RI * W) \oslash W$, where $W = [w_1, w_2, \ldots, w_y]^T$ and the weights are from Step 2 above, and $\oslash$ represents a Hadamard division.

Step B: Find the average of M as (λ_{max}) to compute the consistency index (CI) as

$$\text{CI} = (\lambda_{max} - Y)/(Y - 1). \tag{17}$$

Step C: Compute the CR as $\text{CR} = \text{CI}/r_{index}$, where r_{index}, known as the *random index*, is a standard value computed using

Table 3. Relative Importance Scale

Degree of Importance	Definition
1	Two attributes have equal importance
3	One attribute is slightly more important than the other
5	One attribute is strongly more important than the other
7	One attribute is very strongly more important than the other
9	One attribute is absolutely more important than the other
2, 4, 6, and 8	Intermediate values

a table provided for AHP for a specific value of Y [36,38]. The random index value for $Y = 6$ attributes, as considered in this work, is 1.25. A CR value less than 0.1 indicates good consistency in the RI relations assigned, and the weights can be used with confidence.

Step 3: Preference function calculation (Pref_y)

The preference functions Pref_y represent the evaluation difference between two alternatives (e.g., Alt_1 and Alt_2) w.r.t. a particular attribute y. They are calculated for each of the Y attributes, and they assess the relative contribution of a given alternative concerning a given attribute. Pref_y outputs a preference degree ranging from 0 to 1. PROMETHEE offers six different types of preference functions. The "usual" preference function is the simplest one and is used in this work: it is the difference between values v_{XY} and $v_{X'Y}$ of alternatives Alt_x and $\text{Alt}_{x'}$ (for x, $x' \in X$) w.r.t. an attribute value a_y. Since this is for each of the Y attributes, we get Y separate preference tables. Then, a multiple attribute preference index table is formed using the weighted average of the preference function tables Pref_y, using the weights from Step 2.

Step 4: Calculation of leaving, entering, and net flows

Using the multiple attribute preference index table found in Step 3, we compute the leaving, entering, and net flows. The leaving flow value ϕ^+ is a measure of how much the particular alternative dominates the rest of the alternatives, and the entering flow value ϕ^- denotes how much the rest of the alternatives dominate the alternative. The leaving flow is calculated as the row-wise summation and the entering flow as the column-wise summation of the multiple-attribute preference index table described in Step 3. The net flow $(\phi^+ - \phi^-)$ is a measure of how attractive a particular alternative is. Therefore, the alternatives are ranked by net flow, giving the best rank to the one that has the highest net flow value.

5. CROSS TALK AND FRAGMENTATION-AWARE RMSCA ALGORITHM

Our proposed RMSCA algorithm is given in Algorithm 1. The algorithm begins by computing K ranked paths/cores using Algorithm 2, which takes as input the K shortest paths. For each $k \in K$ and all cores, alternatives are formed and scored using AHP-enabled PROMETHEE. This set of ranked alternatives is used in the outer loop of Algorithm 1 (line 2). The spectrum assignment algorithm is performed inside the loop and relies on a score function based on spectrum blocks on respective cores as described in Algorithm 3. The subsections below detail these two functions.

Algorithm 1. Proposed RMSCA Algorithm

1: **procedure** RMSCA (source, destination, requested BW)
2: Run MADM_route procedure (Algorithm 2) to get ranked route–core alternatives
3: **while** viable spectrum block not found on ranked route–core alternatives and all alternatives not explored **do**
4: Calculate suitable modulation format
5: Create list of candidate spectrum blocks satisfying the continuity and contiguity constraints on that route–core combination
6: Obtain scores for the candidate blocks using Algorithm 3 and sort them in ascending order
7: **while** candidate block in sorted list does not satisfy QoT constraints **do**
8: Compute the impairments and the QoT using Eqs. (3), (1), (2), and (5)
9: **if** QoT is satisfied [Eq. (6)] and existing lightpaths not degraded **then**
10: selected spectrum block = candidate block
11: **else** check next spectrum block
12: **return** current route, core, and selected spectrum block to provision the request

Algorithm 2. MADM Path Selection

1: **procedure** MADM_route (network topology, source, destination, set of cores C, network state)
2: Find K shortest paths from source to destination
3: Obtain core utilization, core fragmentation, number of amplifiers needed, available route BW, energy cost, and the QoT factor information for each path–core alternatives.
4: Apply AHP-enabled PROMETHEE steps to obtain the ranking
5: **return** Ranked $K \times |C|$ path–core alternatives

Algorithm 3. Score Function

1: **procedure** Score_Function (route–core alternative, network status, candidate spectral block)
2: **for** each link e of route L **do**
3: $S_{occ}^{(e)}$ = number of occupied frequency slots on
4: adjacent cores overlapping the spectral block
5: S_{req} = number of frequency slots required to provision the current request
6: $C^{(e)} = [S_{occ}^{(e)} - (S_{req}/2)]^2$
7: $N_F^{(e)}$ = number of fragments created with size less than the required slots
8: E_{Tot} = energy consumed due to using the particular link using Eqs. (10), (13), and (15)
9: Compute weighted multi-objective function
10: $Z^{(e)} = \alpha_1 C^{(e)} + \alpha_2 N_F^{(e)} + \alpha_3 E_{Tot}$
11: Score (candidate block) $= \sum_{e \in L} Z^{(e)}$
12: **return** Score

A. Application of AHP-Enabled PROMETHEE to Routing and Core Selection in SDM-EONs

In this work, AHP-enabled PROMETHEE is used to find the best path and core combination among the available choices as detailed in Algorithm 2. Following the steps explained before, the alternatives here are the path and core combinations. The alternatives for K paths and with $|C|$ cores are denoted as (p_k, c_j) for $k = 1, \ldots, K$ and $j = 1, \ldots, |C|$. The total number of alternatives is $K \times |C|$. In this paper, we use $K = 3$ routes and $|C| = 7$ or $|C| = 12$ cores.

The relevant attributes identified are core utilization (C_U), core fragmentation (C_F), number of amplifiers needed (N_A), number of available frequency slots in the route (S_{Free}), energy cost (E_{Tot}), and the QoT factor (QoT). C_U is included to take into account the uniform utilization of the cores present in a fiber. C_F affects the availability of *contiguous* spectrum resources and thus affects the blocking. N_A depends on the length of the paths, and S_{Free} affects the blocking directly. E_{Tot} captures the energy cost of choosing a particular path and core combination. C_U, C_F, N_A, S_{Free}, E_{Tot}, and QoT for a request using modulation m and a given candidate (path, core) $= (L, c)$ are computed using the following equations:

$$C_U = \sum_{e \in L} \frac{S_m^e}{S}, \tag{18}$$

$$C_F = \sum_{e \in L} F_c^e, \tag{19}$$

$$N_A = \sum_{e \in L} N_s^e, \tag{20}$$

$$S_{\text{Free}} = \sum_{e \in L} \frac{1}{|C|} \sum_{\zeta \in C} (S_m^e)_\zeta, \tag{21}$$

$$E_{\text{Tot}} = E_{\text{BVT}} + E_{\text{OXC}} + E_{\text{EDFA}}, \tag{22}$$

$$QoT = \sum_{e \in L} C_{\text{XT}}^{(c)} + (S - S_m^{(e)})_c + S_{\text{req}}, \tag{23}$$

$$C_{\text{XT}}^{(c)} = \sum_{ac \in N_{ac}} (S - S_m^{(e)})_{ac}, \tag{24}$$

where N_{ac} is the number of adjacent cores for the considered core c. All the above equations use notations having the same meanings as in Section 3 except that they are now defined for a specific core c, wherever used.

As an example, let us assume there are four (path, core) alternatives: (p_1, c_1), (p_2, c_3), (p_2, c_4), and (p_3, c_1). These alternatives are a subset of the considered 21 and 36 alternatives (for 7-core and 12-core MCFs, respectively, and three shortest paths) in this work and are chosen only to illustrate the algorithm's working. Table 4 shows the decision table containing information about the alternatives, attributes, and corresponding data. Higher values of C_U and S_{Free} and lower values of C_F, N_A, E_{Tot}, and QoT are desired. The relevant system and fiber parameters are given in Table 7 in Section 6.

Table 4. Decision Table

Alternatives	C_U	C_F	N_A	S_{Free}	E_{Tot}	QoT
(p_1, c_1)	0.625	30	8	96	92	1740
(p_2, c_3)	0.9375	74	11	148	127	1405
(p_2, c_4)	0.828	132	11	148	127	1860
(p_3, c_1)	0.475	62	14	117	164	2587

Following with this example, we can compute the attribute weights using the RI matrix, resulting in

$$\text{RI} = \begin{array}{c} \text{Attribute} \\ C_U \\ C_F \\ N_A \\ S_{\text{Free}} \\ E_{\text{Tot}} \\ QoT \end{array} \begin{array}{c} \begin{array}{cccccc} C_U & C_F & N_A & S_{\text{Free}} & E_{\text{Tot}} & QoT \end{array} \\ \begin{bmatrix} 1 & 1/3 & 3 & 1 & 5 & 1/4 \\ 3 & 1 & 5 & 3 & 7 & 1/3 \\ 1/3 & 1/5 & 1 & 1/3 & 3 & 1/6 \\ 1 & 1/3 & 3 & 1 & 5 & 1/4 \\ 1/5 & 1/7 & 1/3 & 1/5 & 1 & 1/7 \\ 4 & 3 & 6 & 4 & 7 & 1 \end{bmatrix} \end{array}. \tag{25}$$

To obtain this, C_U is considered slightly more important than the N_A required; hence, a value of three is assigned. Accordingly, the reciprocal 1/3 is given to N_A vs C_U matrix entry. Note that these assignments illustrate only the proposed AHP-enabled PROMETHEE for path selection: in real practice, decision makers may assign values on a scale of 1–9 according to Table 3 based on their expertise toward solving the particular problem.

As explained in Section 4, the geometric means of the attributes are calculated as

for C_U: $(1 * 1/3 * 3 * 1 * 5 * 1/4)^{1/6} = 1.037$,
for C_F: $(3 * 1 * 5 * 3 * 7 * 1/3)^{1/6} = 2.172$,
for N_A: $(1/3 * 1/5 * 1 * 1/3 * 3 * 1/6)^{1/6} = 0.472$,
for S_{Free}: $(1 * 1/3 * 3 * 1 * 5 * 1/4)^{1/6} = 1.037$,
for E_{Tot}: $(1/5 * 1/7 * 1/3 * 1/5 * 1 * 1/7)^{1/6} = 0.254$,
for QoT: $(4 * 3 * 6 * 4 * 7 * 1)^{1/6} = 3.554$.

The sum of these geometric means is 8.526. The corresponding weights of the attributes are obtained by dividing their geometric means by the sum:

$w_{CU} = 1.037/8.526 = 0.1217$,
$w_F = 2.172/8.526 = 0.2546$,
$w_{N_A} = 0.472/8.526 = 0.0553$,
$w_{S_{\text{Free}}} = 1.037/8.526 = 0.1217$,
$w_{E_{\text{Tot}}} = 0.254/8.526 = 0.0298$,
$w_{QoT} = 3.554/8.526 = 0.4167$.

Putting these weights into a vector, we denote $W = [0.1217, 0.2546, 0.0553, 0.1217, 0.0298, 0.4167]^T$. The CR computations following the steps given in Section 4 are given as below.

Step A: Derive the vector M:

$$M = \begin{bmatrix} 0.7478/0.1217 = 6.1454 \\ 1.6095/0.2546 = 6.3203 \\ 0.3464/0.0553 = 6.2550 \\ 0.7478/0.1217 = 6.1454 \\ 0.1928/0.0298 = 6.4629 \\ 2.6954/0.4167 = 6.4682 \end{bmatrix}. \tag{26}$$

Step B: The value of $\lambda_{\max}$ is 6.2995. The CI value is computed as $CI = (6.2995 - 6)/(6 - 1) = 0.0599$.

Step C: The CR value is $0.0599/1.25 = 0.0479$. This is much less than 0.1, indicating good consistency in the RI relations assigned, and the weights can be accepted.

Next, the preference values (Pref_y) resulting from the pairwise comparisons of the alternatives with respect to each attribute are found. Table 5 shows these values for the C_U attribute; similar preference tables are formed for the remaining attributes. Pairwise comparison means that when an alternative Alt_i dominates another alternative Alt_j, a 1 is assigned to matrix element (i, j), and 0 is assigned to element (j, i). However, if two alternatives are equal, no dominance exists and 0 is assigned in both cases. Using the four preference tables for the $X = 4$ alternatives, a multiple attribute preference index table is formed, as shown in Table 6.

The leaving, entering, and net flows are calculated next. The leaving flow is computed as the row-wise summation and the entering flow as the column-wise summation of the preference values of Table 6. Net flow (ϕ) is calculated as the difference between leaving and entering flows, i.e., $(\phi^+ - \phi^-)$, which come out to be 0.9754, 1.604, −0.8154, and −1.764 for the example shown. Based on these ϕ values, the alternatives are ranked in descending order, and the best alternative is the first one. Hence, the ranking of the alternatives becomes (p_2, c_3), (p_1, c_1), (p_2, c_4), (p_3, c_1), with (p_2, c_3) being the best choice.

B. Spectrum Assignment

The next step is to find the spectral blocks satisfying the continuity and contiguity conditions for the particular route–core combination being considered. The score function algorithm, Algorithm 3, is called Algorithm 1 for the candidate blocks, and they are sorted in ascending order of their scores in line 6. All spectrum blocks of the size required for the data rate and modulation format selected that obey the continuity and contiguity constraints of the EONs are considered candidate blocks. The QoT is checked starting with the first candidate block. If it does not satisfy the threshold criterion in Eq. (6) or unduly degrades other established lightpaths, the search proceeds toward the next spectrum block. However, if Eq. (6) is satisfied, then the current candidate block is selected. Hence, the loop at line 7 of Algorithm 1 continues until a QoT-satisfying block is found. Since the scores already incorporate the XT aspect as one term, we can be assured that the found block from the sorted set is one of the better choices w.r.t. XT satisfaction, and there is no need to continue the search for other spectrum blocks.

Table 5. Preference Values for the C_U Attribute

CU (0.1217)	(p_1, c_1)	(p_2, c_3)	(p_2, c_4)	(p_3, c_1)
(p_1, c_1)	–	0	0	1
(p_2, c_3)	1	–	1	1
(p_2, c_4)	1	0	–	1
(p_3, c_1)	0	0	0	–

Table 6. Preference Relations and the Ranks of Alternatives

	(p_1, c_1)	(p_2, c_3)	(p_2, c_4)	(p_3, c_1)	ϕ^+
(p_1, c_1)	–	0.3485	0.7652	0.8869	2.0006
(p_2, c_3)	0.6601	–	0.793	0.754	2.2071
(p_2, c_4)	0.2434	0	–	0.754	0.9974
(p_3, c_1)	0.1217	0.2546	0.2546	–	0.6309
ϕ^-	1.0252	0.6031	1.8128	2.3949	

We define a weighted multi-objective function that computes a score for the feasible candidate spectrum block, returned by Algorithm 3. This score is calculated for the entire route–core alternative and considers the number of occupied slots surrounding the candidate block on adjacent cores, and the amount of fragmentation incurred from selecting that block on that core and on that route. As seen from Algorithm 3, for each link, the first term, $C^{(e)}$, denotes the score value considering XT, the second term, $N_F^{(e)}$, denotes the score value relating to the additional fragmentation caused by selecting that particular spectral block, and the third term, E_{Tot}, calculates the energy consumption. Depending on the weights chosen, the algorithm can emphasize a lower expected XT, fragmentation-causing capability, or energy cost when considering the whole route. This spectrum selection scheme using scores is named as Score Fit (SF) in this work.

To see how the $N_F^{(e)}$ term captures the spectral block's fragmentation-causing capability when compared to classical spectrum schemes [39], consider a link's spectrum status [ABCD111HIJKLM11PQRST11], where a "1" denotes an occupied slot, and the letters are position indicators denoting available slots. Assume three frequency slots are required to accommodate the current traffic request, i.e., $S_{\text{req}} = 3$. Then, the candidate blocks are [ABC], [BCD], [HIJ], [IJK], [JKL], [KLM], [PQR], [QRS], and [RST]. Assume that these candidates satisfy the continuity constraint. The classical spectrum allocation algorithms, First Fit (FF), Last Fit, Exact Fit, and Best Fit (BF) [40], would choose [ABC], [RST], [ABC], and [ABC], respectively. However, these blocks create fragments of sizes 1, 2, 1, and 1, respectively, which is wasteful w.r.t. future traffic. However, the $N_F^{(e)}$ term would encourage the selection of [HIJ] or [KLM] as they leave zero fragments with sizes less than S_{req}, thus leaving bigger blocks of contiguous available slots.

The complexity of the proposed Algorithm 1 is $O(KS|C|)$, where K is the number of routes considered, S is the number of frequency slots, and $|C|$ is the number of cores.

6. NETWORK RESULTS

The proposed algorithm is tested on two network topologies, the 11-node and 52-link COST 239 and the 14-node and 21-link NSFNET, using a 7-core MCF on each link. The NSFNET is additionally tested with 12-core links to check the robustness of the algorithms. Both networks have a wide diversity of link distances (200–2400 km), which is essential while considering the inclusion of PLI. This work assumes a 4 THz optical spectrum per core for both networks. Each frequency slot of a core supports 12.5 GHz transmission. The system and fiber parameters used in the current work are given in Table 7.

A Poisson traffic distribution model is used to generate 100,000 requests for varying loads with data rates uniformly

Table 7. System and Fiber Parameters Used [31]

Parameters	Values
Fiber loss, dB/km	0.2
Dispersion, ps/nm/km	17
Dispersion slope, ps/nm^2/km	0.067
Nonlinear coefficient, 1/W/km	1.2
Channel launch power, dBm	0
Number of channels	Variable
Optical bandwidth, THz	4
Slot bandwidth, GHz	12.5
α_1	0.4
α_2	0.4
α_3	0.2
K	3
$\|C\|$	7, 12

distributed in [50,300] Gbps. A request comprises a source node, a destination node, and requested data rate. Modulation selection is distance adaptive, and the modulation formats considered are BPSK, QPSK, 8-QAM, 16-QAM, and 32-QAM; the threshold SNRs are adopted from [41]. The algorithm's effectiveness is measured by calculating the blocking probability (BP), BW BP (BBP), network fragmentation (F_{net}) computed using Eq. (7), and total energy consumption (E_{NET}). The BP and BBP are given by

$$\mathrm{BP} = \frac{\text{Number of blocked requests}}{\text{Total number of requests}} \tag{27}$$

and

$$\mathrm{BBP} = \frac{\text{Amount of blocked bandwidth}}{\text{Total amount of requested bandwidth}}. \tag{28}$$

The next sections show our simulation results where a 95% confidence interval is drawn as error bars around each mean value over five trials. In all the results, the conventional KSP routing with FF spectrum assignment algorithm is subjected to the QoT constraint for a fair comparison with the proposed approach. Our results are also compared with a recently published impairment-aware RMSCA algorithm described in [18]. The authors proposed a DI-aware RMSCA algorithm. However, SPM impairment was not considered in their work; hence, for a fair comparison, our proposed algorithms are also simulated without the SPM effect whenever compared with the DI-aware algorithm.

A. Performance Analysis, Seven-Core MCF: Blocking Probability

We begin by analyzing the algorithms' performance when operating in networks where all links use 7-core MCFs. The 7-core fiber has a core at the center and six cores surrounding it.

Figures 1 and 2 compare the BP obtained using the benchmark KSP and the proposed MADM routing under FF spectrum allocation and the proposed SF approach for the two networks considered, respectively.

The results show that the MADM SF obtains the lowest BP among the considered algorithms. For a given routing scheme (KSP or MADM), the SF performs better than the benchmark FF. And for a given spectrum allocation (FF or SF), the MADM routing aids in obtaining lower blocking. This behavior is because KSP considers only distance, whereas MADM-based routing uses a holistic approach, including blocking-affecting metrics. The performance of KSP SF is comparable with MADM FF but still performs better than the routing and spectrum benchmark (KSP using FF). This tells us that the improvement obtained by using the improved spectrum allocation algorithm SF over FF is similar to the improvement obtained by using the improved routing algorithm MADM over KSP. Similar observations can be drawn from the blocking behavior in the NSFNET and COST 239 networks.

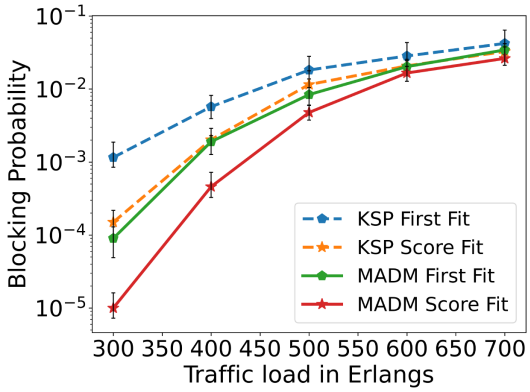

Fig. 1. Blocking probabilities for the KSP First Fit, KSP Score Fit, MADM First Fit, and MADM Score Fit in a 7-core NSFNET.

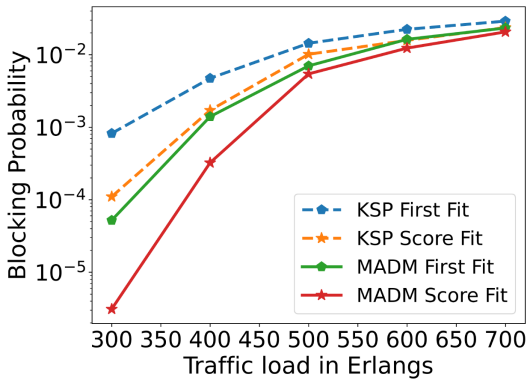

Fig. 2. Blocking probabilities for the KSP First Fit, KSP Score Fit, MADM First Fit, and MADM Score Fit in a 7-core COST 239.

Figure 3 shows the BP comparison between our proposed algorithm and the DI-aware algorithm. The BP is slightly lower than in Fig. 1 since the SPM effect is absent. The DI-aware algorithm uses KSP routing; hence, we show the KSP case with our SF and the MADM routing with SF. MADM SF offers significantly lower blocking, and even KSP SF offers slightly better performance than the DI-aware scheme. This is because the SF is more concerned with XT than with the other impairments considered in the MADM routing decision; hence, MADM SF performed better than the KSP SF when compared to the DI-aware scheme.

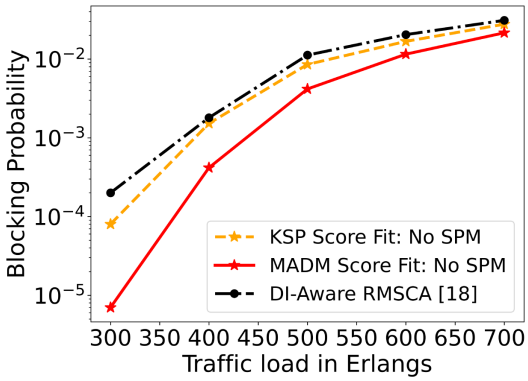

Fig. 3. Blocking probabilities for the KSP Score Fit, MADM Score Fit, and the DI-aware RMSCA algorithm in a 7-core NSFNET.

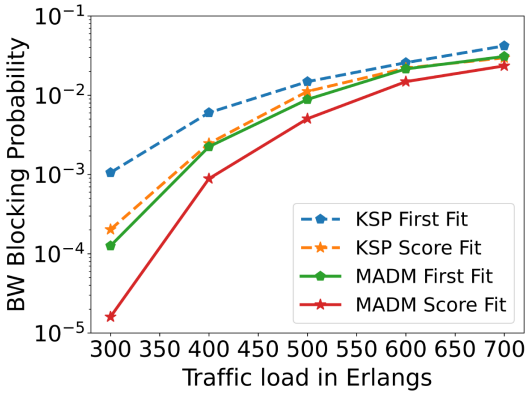

Fig. 4. BW blocking probabilities for the KSP First Fit, KSP Score Fit, MADM First Fit, and MADM Score Fit in a 7-core NSFNET.

B. Performance Analysis, Seven-Core MCF: Bandwidth Blocking Probability

Since SDM-EONs are expected to carry high amounts of data, analysis of BBP gives better insight into the network performance than the BP that treats all requests the same irrespective of their size [3]. Figures 4 and 5 show the BBP for the benchmark KSP and the proposed MADM routing with FF and SF spectrum allocation for the two networks, respectively. Results show that MADM SF obtains the lowest BBP among the considered algorithms. This is because, at any given time, the SF tries to find a block that balances the XT and fragmentation-causing capabilities. As a result, the chance of successful allocation is higher in the proposed approach despite changes in the request sizes. Furthermore, with any given candidate spectral block, the algorithm considers how much fragmentation it could cause that can lead to the possibility of rejection of future bigger-sized requests. Similar performance conclusions as those of BP can be drawn regarding the relative performance of other approaches in NSFNET and COST 239 networks.

C. Performance Analysis, Seven-Core MCF: Energy Consumption

Figure 6 shows the energy consumption (kW) in the NSFNET network as a function of traffic load when using the benchmark

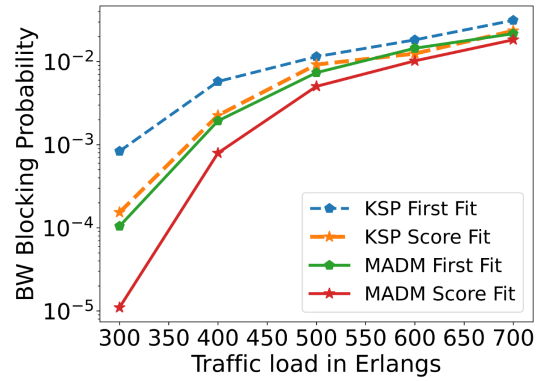

Fig. 5. BW blocking probabilities for the KSP First Fit, KSP Score Fit, MADM First Fit, and MADM Score Fit in a 7-core COST 239.

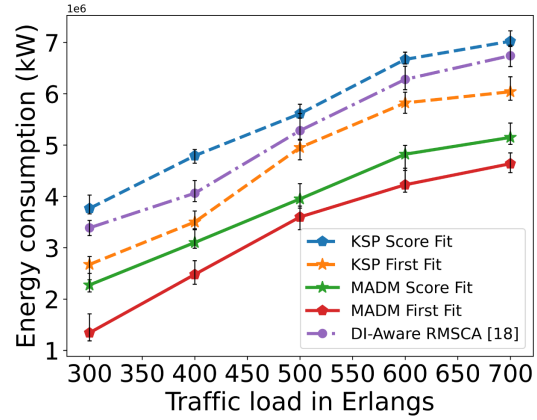

Fig. 6. Total energy consumption for KSP First Fit, KSP Score Fit, MADM First Fit, MADM Score Fit, and the DI-aware RMSCA algorithm in a 7-core NSFNET.

KSP and the proposed MADM routing under FF and SF spectrum allocation methods. As expected, the consumption increases with increasing load. Despite similar BP and BBP performances for KSP SF and MADM SF, they vary in energy consumption. MADM-based RMSCA solutions are more energy efficient than KSP-based ones. Including energy cost via an attribute while applying PROMETHEE in the MADM routing decision stage has been more beneficial than in the spectrum allocation stage for the considered C-band operation. MADM FF shows lower energy consumption than MADM SF due to its higher blocking. Similar reasoning goes for the performance differences between KSP FF and KSP SF.

The DI-aware approach of [18] did not consider energy consumption. Hence, we compute and plot the consumption here by subjecting the algorithm to the formulas [Eqs. (10)–(15)] used for our proposed methods. Results show that the DI-aware approach causes more energy consumption than the proposed approaches—an algorithm being impairment aware is unrelated to how energy efficient it is.

D. Performance Analysis, Seven-Core MCF: Network Fragmentation

Figure 7 shows the network fragmentation that occurs over different traffic loads for KSP and MADM routing under FF

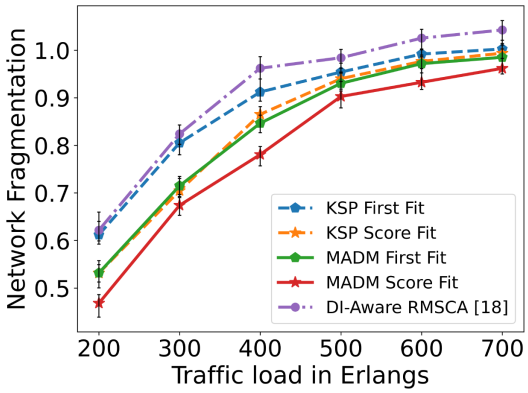

Fig. 7. Network fragmentation for the KSP First Fit, KSP Score Fit, MADM First Fit, MADM Score Fit, and the DI-aware RMSCA algorithm in a 7-core NSFNET.

and SF spectrum allocation for the NSFNET network. In addition, we also analyze the fragmentation resulting when the DI-aware published benchmark is used. The fragmentation metric can take values ranging from 0 to ∞ [32].

The MADM SF maintains lower fragmentation levels than the other algorithms for all traffic loads tested. The KSP FF compactly allocates the spectrum at any given time, but as seen in Section 5, the SF better quantifies and allocates the spectrum. This causes the proposed SF to perform better. In addition, the use of fragmentation as an attribute in the MADM route selection process helps to improve the performance further. The DI-aware approach did not consider fragmentation. Hence, we compute and plot the metric here by subjecting the algorithm to the formula [Eq. (7)] used for our proposed methods. The algorithm results in higher fragmentation than the KSP FF. This is because the DI-aware approach minimizes the impairments' impact and does not include fragmentation in the spectrum allocation design process. Instead, it uses KSP routing; hence, considering the spectrum part alone, the FF is naturally better at reducing fragmentation than the DI-aware allocation.

E. Performance Analysis: 12-Core MCF

Figures 8–11 show the BP, BBP, network fragmentation, and energy consumption, respectively, in a 12-core-based NSFNET. A ring-structured 12-core fiber is assumed for all simulations [42].

Figure 8 shows that MADM SF obtains the lowest BP among the algorithms tested for similar reasons as in the case of 7-core MCF. Similarly, the KSP SF and MADM FF give close results. However, the performance difference between the algorithms is smaller than in the 7-core case. The reason is that the number of neighbors in the ring-structured 12-core MCF link is less than in the 7-core type; hence, the XT experienced by a signal is lower. Since the algorithms are XT aware, they might show a higher performance advantage when the XT is stronger. However, the algorithms still perform better than the KSP FF benchmark due to including holistic network features in routing and spectrum allocation decisions.

Conclusions drawn from the results in Fig. 9 are similar to those for the 7-core MCF network shown in Fig. 4. The

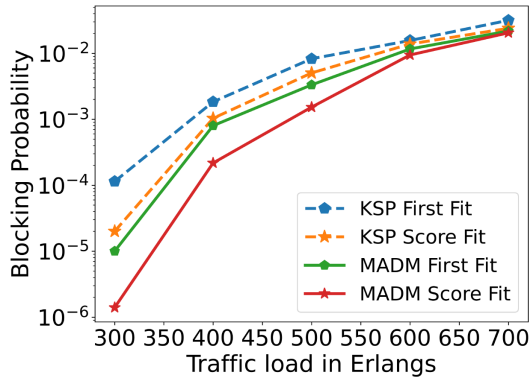

Fig. 8. Blocking probabilities for the KSP First Fit, KSP Score Fit, MADM First Fit, and MADM Score Fit in a 12-core NSFNET.

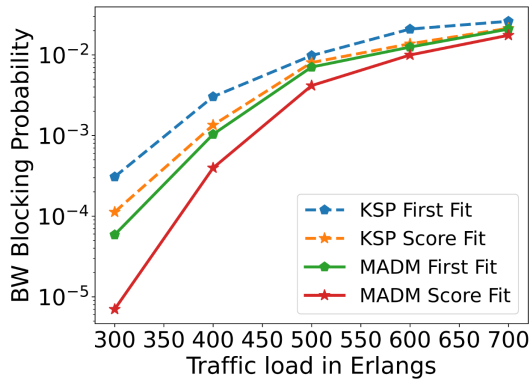

Fig. 9. BW blocking probabilities for the KSP First Fit, KSP Score Fit, MADM First Fit, and MADM Score Fit in a 12-core NSFNET.

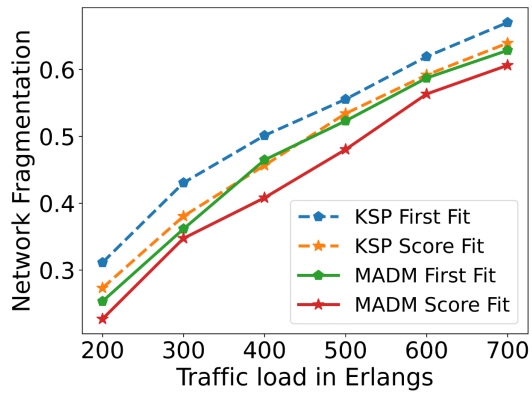

Fig. 10. Network fragmentation for the KSP First Fit, KSP Score Fit, MADM First Fit, MADM Score Fit, and the DI-aware RMSCA algorithm in a 12-core NSFNET.

proposed methods maintained lower BW blocking than the KSP FF with MADM SF being the best. Figure 10 shows the obtained 12-core MCF network fragmentation for the proposed algorithms. Similar to the 7-core case, the SF aids in a better quantification of the network fragments before deciding the RMSCA solution and hence provides lower fragmentation when combined with MADM routing. Figure 11 shows the energy consumption in a 12-core MCF network; the MADM

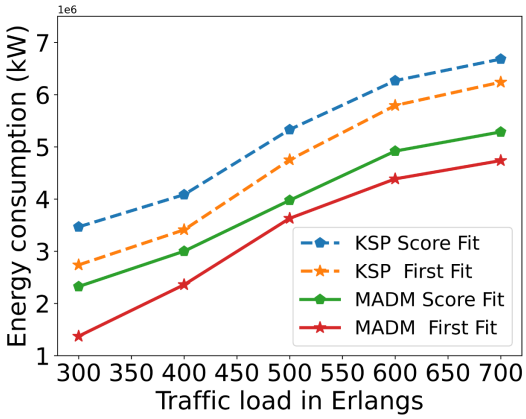

Fig. 11. Total energy consumption for KSP First Fit, KSP Score Fit, MADM First Fit, MADM Score Fit, and the DI-aware RMSCA algorithm in a 12-core NSFNET.

approaches maintain lower energy consumption than the other approaches as the traffic loads increase.

7. CONCLUSIONS

An impairment-aware, fragmentation-aware, and energy-efficient RMSCA algorithm for C-band SDM-EONs is proposed in this paper. The present work considers the XT, Kerr NLIs such as SPM and XPM, and also ASE noise encountered by the signal along the chosen network path. Novelty is introduced in the form of new routing and new spectrum allocation processes. A MADM-based routing that considers relevant network aspects is used to rank the candidate routes for traffic requests. In the spectrum allocation part, a score-based approach uses a weighted function that qualitatively incorporates the effects of the expected XT and the expected fragmentation on existing and upcoming traffic while maintaining lower energy consumption levels. To the best of our knowledge, this is the first work that considers all impairments in SDM-EONs while also being fragmentation and energy aware.

The simulations are performed on two diverse network topologies, NSFNET and COST 239 with 7- and 12-core MCF links, and the results of BP, BBP, network fragmentation, and energy consumption are analyzed. The novel combination of MADM routing and score function spectrum assignment performs significantly better than conventional and published benchmarks for all cases tested. More network metrics can be incorporated into the MADM attributes for future work. Accordingly, the alternatives can be made diverse to make the final selection relevant to the network goal to be optimized. The reduction in the number of alternatives may also be tried but in a way that can still affect the network status positively upon getting selected by the MADM method. The allowance of optical relays would also be interesting to consider.

REFERENCES

1. "CISCO annual Internet report (2018–2023) white paper" (CISCO, 2020).
2. J. L. Ravipudi and M. Brandt-Pearce, "Impairment-and fragmentation-aware dynamic routing, modulation and spectrum allocation in C+L band elastic optical networks using Q-learning," Opt. Switch. Netw. **47**, 100717 (2023).
3. Í. Brasileiro, L. Costa, and A. Drummond, "A survey on challenges of spatial division multiplexing enabled elastic optical networks," Opt. Switch. Netw. **38**, 100584 (2020).
4. K. Christodoulopoulos, I. Tomkos, and E. A. Varvarigos, "Elastic bandwidth allocation in flexible OFDM-based optical networks," J. Lightwave Technol. **29**, 1354–1366 (2011).
5. H. Liu, Q. Xiong, and Y. Chen, "Routing core and spectrum allocation algorithm for inter-core crosstalk and energy efficiency in space division multiplexing elastic optical networks," IEEE Access **8**, 70453–70464 (2020).
6. S. Fujii, Y. Hirota, H. Tode, and T. Watanabe, "On-demand routing and spectrum allocation for energy-efficient AoD nodes in SDM-EONs," J. Opt. Commun. Netw. **9**, 960–973 (2017).
7. J. Halder, S. Paira, T. Acharya, and U. Bhattacharya, "Design of a novel XT-aware energy and spectrum efficient RSCA scheme in offline SDM-EON," Opt. Fiber Technol. **63**, 102502 (2021).
8. J. Halder, T. Acharya, and U. Bhattacharya, "On crosstalk aware energy and spectrum efficient survivable RSCA scheme in offline SDM-EON," J. Netw. Syst. Manage. **30**, 6 (2022).
9. H. Tode and Y. Hirota, "Routing, spectrum, and core and/or mode assignment on space-division multiplexing optical networks," J. Opt. Commun. Netw. **9**, A99–A113 (2017).
10. M. Yang, Y. Zhang, and Q. Wu, "Routing, spectrum, and core assignment in SDM-EONS with MCF: node-arc ILP/MILP methods and an efficient XT-aware heuristic algorithm," J. Opt. Commun. Netw. **10**, 195–208 (2018).
11. S. Zhang and K. L. Yeung, "Dynamic service provisioning in space-division multiplexing elastic optical networks," J. Opt. Commun. Netw. **12**, 335–343 (2020).
12. R. Zhu, A. Samuel, P. Wang, S. Li, L. Li, P. Lv, and M. Xu, "Survival multipath energy-aware resource allocation in SDM-EONs during fluctuating traffic," J. Lightwave Technol. **39**, 1900–1912 (2020).
13. S. Zhang, K.-L. Yeung, and A. Jin, "LBFA: a load-balanced and fragmentation-aware resource allocation algorithm in space-division multiplexing elastic optical networks," Photonics **8**, 456 (2021).
14. X. Li, J. Yuan, L. Yang, Q. Zhang, and Z. Yu, "A crosstalk- and fragmentation-aware RMSCA strategy in SDM-EONs based on aligned prime-partition of spectrum resources," Opt. Fiber Technol. **72**, 102978 (2022).
15. A. Samuel, Y. Zhang, and R. Zhu, "Deadline-aware multicast resource allocation in SDM-EONs with fluctuating delay-sensitive traffic," J. Lightwave Technol. **40**, 5355–5368 (2022).
16. S. Zhang and K. L. Yeung, "Revisiting the modulation format selection problem in crosstalk-aware SDM-EONs," Comput. Netw. **221**, 109524 (2023).
17. J. Ravipudi and M. Brandt-Pearce, "A score function heuristic for crosstalk- and fragmentation-aware dynamic routing, modulation, core, and spectrum allocation in SDM-EONs," in *IEEE Future Networks World Forum*, Montreal, Québec, Canada, 2022.
18. J. Su, J. Zhang, J. Wang, D. Ren, J. Hu, and J. Zhao, "Dynamic impairment-aware RMCSA in multi-core fiber-based elastic optical networks," Opt. Commun. **518**, 128361 (2022).
19. E. Pourkarimi and A. G. Rahbar, "Novel fragmentation-aware algorithms in space division multiplexing elastic optical networks," Opt. Fiber Technol. **66**, 102655 (2021).
20. K. Walkowiak, A. Wlodarczyk, and M. Klinkowski, "Effective worst-case crosstalk estimation for dynamic translucent SDM elastic optical networks," in *IEEE International Conference on Communications (ICC)* (IEEE, 2019).
21. Y. Zhao, L. Hu, R. Zhu, X. Yu, X. Wang, and J. Zhang, "Crosstalk-aware spectrum defragmentation based on spectrum compactness in space division multiplexing enabled elastic optical networks with multicore fiber," IEEE Access **6**, 15346–15355 (2018).
22. D. Kumar and R. Ranjan, "Optimal design for crosstalk analysis in 12-core 5-LP mode homogeneous multicore fiber for different lattice structure," Opt. Fiber Technol. **41**, 95–103 (2018).
23. E. E. Moghaddam, H. Beyranvand, and J. A. Salehi, "Crosstalk-aware resource allocation in survivable space-division-multiplexed elastic optical networks supporting hybrid dedicated and shared path protection," J. Lightwave Technol. **38**, 1095–1102 (2019).

24. F. Tang, G. Shen, and G. N. Rouskas, "Crosstalk-aware shared backup path protection in multi-core fiber elastic optical networks," J. Lightwave Technol. **39**, 3025–3036 (2021).
25. M. Klinkowski and G. Zalewski, "Dynamic crosstalk-aware lightpath provisioning in spectrally–spatially flexible optical networks," J. Opt. Commun. Netw. **11**, 213–225 (2019).
26. R. Zhu, A. Samuel, P. Wang, S. Li, B. K. Oun, L. Li, P. Lv, M. Xu, and S. Yu, "Protected resource allocation in space division multiplexing-elastic optical networks with fluctuating traffic," J. Netw. Comput. Appl. **174**, 102887 (2021).
27. R. Proietti, L. Liu, R. P. Scott, B. Guan, C. Qin, T. Su, F. Giannone, and S. J. B. Yoo, "3D elastic optical networking in the temporal, spectral, and spatial domains," IEEE Commun. Mag. **53**(2), 79–87 (2015).
28. R. A. Oliveira, D. Rosário, E. Cerqueira, and H. Oliveira, "Machine learning assisted traffic-aware approach to path assignment in SDM-EONs," in *Anais do XL Simpósio Brasileiro de Redes de Computadores e Sistemas Distribudos* (SBC, 2022), pp. 29–42.
29. J. Pinto-Ros, F. Calderón, A. Leiva, G. Hermosilla, A. Beghelli, D. Bórquez-Paredes, A. Lozada, N. Jara, R. Olivares, and G. Saavedra, "Resource allocation in multicore elastic optical networks: a deep reinforcement learning approach," arXiv, arXiv:2207.02074 (2022).
30. Y. Xu, E. Agrell, and M. Brandt-Pearce, "Cross-layer static resource provisioning for dynamic traffic in flexible grid optical networks," J. Opt. Commun. Netw. **13**, 1–13 (2021).
31. D. Semrau, E. Sillekens, R. I. Killey, and P. Bayvel, "A modulation format correction formula for the Gaussian noise model in the presence of inter-channel stimulated Raman scattering," J. Lightwave Technol. **37**, 5122–5131 (2019).
32. P. Lechowicz, M. Tornatore, A. Włodarczyk, and K. Walkowiak, "Fragmentation metrics and fragmentation-aware algorithm for spectrally/spatially flexible optical networks," J. Opt. Commun. Netw. **12**, 133–145 (2020).
33. M. Ju, F. Zhou, S. Xiao, and Z. Zhu, "Power-efficient protection with directed-cycles for asymmetric traffic in elastic optical networks," J. Lightwave Technol. **34**, 4053–4065 (2016).
34. G.-H. Tzeng and J.-J. Huang, *Multiple Attribute Decision Making: Methods and Applications* (CRC Press, 2011).
35. R. Rao and B. K. Patel, "Decision making in the manufacturing environment using an improved PROMETHEE method," Int. J. Prod. Res. **48**, 4665–4682 (2010).
36. R. V. Rao, "Multiple attribute decision making in the manufacturing environment," in *Decision Making in Manufacturing Environment Using Graph Theory and Fuzzy Multiple Attribute Decision Making Methods* (Springer, 2013), pp. 1–5.
37. J.-P. Brans, P. Vincke, and B. Mareschal, "How to select and how to rank projects: the PROMETHEE method," Eur. J. Oper. Res. **24**, 228–238 (1986).
38. R. L. Saaty, "The analytic hierarchy process—what it is and how it is used," Math. Model. **9**, 161–176 (1987).
39. B. Chatterjee and E. Oki, *Elastic Optical Networks: Fundamentals, Design, Control, and Management* (CRC Press, 2020).
40. F. S. Abkenar, A. G. Rahbar, and A. Ebrahimzadeh, "Best fit (BF): a new spectrum allocation mechanism in elastic optical networks (EONs)," in *8th International Symposium on Telecommunications (IST)* (IEEE, 2016), pp. 24–29.
41. J. Zhao, H. Wymeersch, and E. Agrell, "Nonlinear impairment-aware static resource allocation in elastic optical networks," J. Lightwave Technol. **33**, 4554–4564 (2015).
42. S. Matsuo, Y. Sasaki, T. Akamatsu, I. Ishida, K. Takenaga, K. Okuyama, K. Saitoh, and M. Kosihba, "12-core fiber with one ring structure for extremely large capacity transmission," Opt. Express **20**, 28398–28408 (2012).